Available online at www.sciencedirect.com
SCIENCE DIRECT®
Journal of Nuclear Materials 329–333 (2004) 31–38
journal of nuclear materials
www.elsevier.com/locate/jnucmat

ITER nuclear components, preparing for the construction and R&D results

K. Ioki [a,*], M. Akiba [b], P. Barabaschi [a], V. Barabash [a], S. Chiocchio [a], W. Daenner [c], F. Elio [a], M. Enoeda [b], K. Ezato [b], G. Federici [a], A. Gervash [d], D. Grebennikov [d], L. Jones [c], S. Kajiura [b], V. Krylov [d], T. Kuroda [b], P. Lorenzetto [c], S. Maruyama [a], M. Merola [c], N. Miki [b], M. Morimoto [a], M. Nakahira [b], J. Ohmori [b], M. Onozuka [b], V. Rozov [a], K. Sato [b], Yu. Strebkov [d], S. Suzuki [b], V. Tanchuk [d], R. Tivey [a], Yu. Utin [a]

[a] *ITER International Team, Boltzmannstraße 2, D85748 Garching, Germany*
[b] *JAPT, JAERI, Naka Establishment, Naka-machi, Naka-gun, Ibaraki-ken 311-0193, Japan*
[c] *EUPT, EFDA-CSU, Boltzmannstraße 2, 85748 Garching, Germany*
[d] *RFPT, NTC Sintez, Efremov Inst., 189631 Metallostroy, St. Petersburg, Russia*

Abstract

Progress has been made in the preparation of the procurement specifications for key nuclear components of ITER. Detailed design of the vacuum vessel (VV) and in-vessel components is being performed to consider fabrication methods and non-destructive tests (NDT). R&D activities are being carried out on vacuum vessel UT inspection with waves launched at an angle of 20° or 30°, on flow distribution tests of a two-channel model, on fabrication and testing of FW mock-ups and panels, on the blanket flexible support as a complete system including the housing, on the blanket co-axial pipe connection with guard vacuum for leak detection, and on divertor vertical target prototypes. The results give confidence in the validity of the design and identify possibilities of attractive alternate fabrication methods.

1. Introduction

The ITER Project is now moving towards its construction phase. The design of the nuclear components such as the first wall (FW), blanket, divertor and VV has progressed considering the fabrication method, reliability and maintainability. Procurement specifications for the VV are now being prepared because the VV delivery is on the critical path and the fabrication is required to start early in construction. R&D activities have been continued to confirm the design validity and to develop cost-saving fabrication methods. The applicable codes and standards are tentatively assumed by the ITER Project. It is planned to negotiate flexibly with regulators about the applicable codes and standards after the ITER site selection.

2. Vacuum vessel

2.1. Vacuum vessel design and R&D

The VV remains a double-walled torus-shaped structure (as shown in Fig. 1) of SS 316L(N)-IG (ITER Grade) [1]. The main vessel consists of inner and outer shells, poloidal and toroidal ribs and in-wall shielding. Flexible support housings and keys are welded to the

* Corresponding author. Tel.: +49-89 3299 4428; fax: +49-89 3299 4422.
E-mail address: iokik@itereu.de (K. Ioki).

0022-3115/$ - see front matter © 2004 Elsevier B.V. All rights reserved.
doi:10.1016/j.jnucmat.2004.04.003

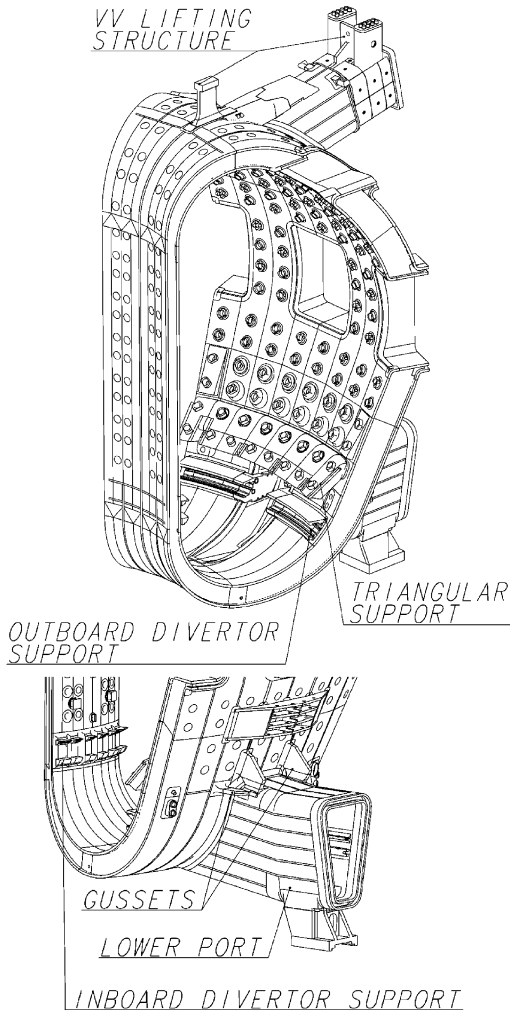

Fig. 1. The ITER vacuum vessel.

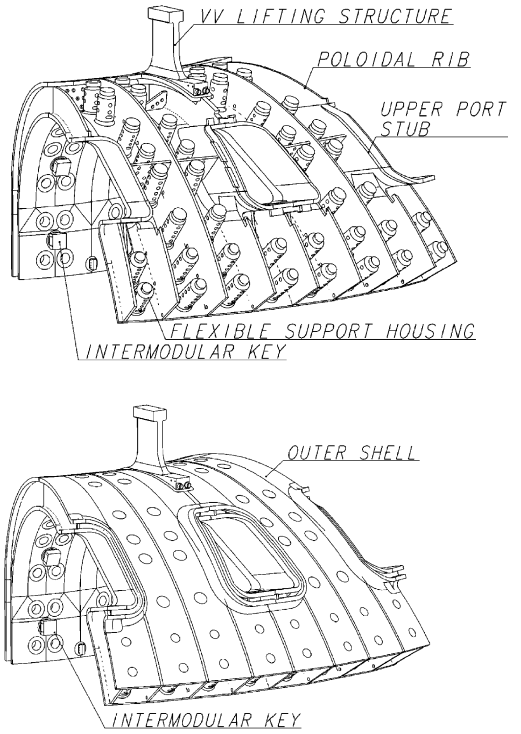

Fig. 2. Double-wall vessel with keys and flexible support housings.

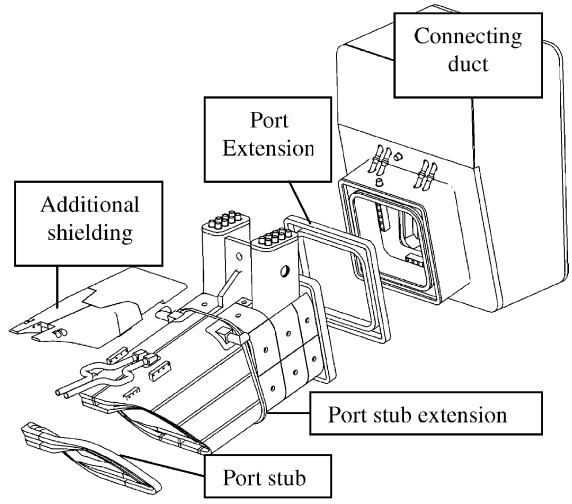

Fig. 3. Upper port structure.

vessel shells, as shown in Fig. 2, since the blanket modules are directly supported by the VV. Electron beam welding is used for joints between the inner shell and these structures. The layout of welds on the inner and outer shells is very tight considering accessibility for welding and non-destructive examination requirements defined in the design codes. The triangular support (see Fig. 1) plays an important role in the plasma vertical stability control during minor disruptions, and its position and configuration is optimized based on the plasma vertical stability analysis. Detailed design has been developed for the triangular support considering the fabrication method and the structural integrity. Additional structures for lifting during the assembly have been designed at two locations in the upper region of the vessel, as shown in Fig. 1.

Detailed design of the upper port (see Fig. 3) has progressed to take into account the fabrication method and the assembly. The locations of the upper port field joints and the layout of the connecting cooling pipes have been optimized considering the welding distortion during the port assembly and the assembly schedule of the blanket cooling pipes. The volume in the interspace between the inner and outer shells in field joint regions is

now fully isolated to permit independent leak checking during the VV assembly. The VV is supported at the lower ports on the cryostat floor, and horizontal and vertical gussets (100 mm thick) reinforcing the lower port stub region (see Fig. 1) have been optimized based on analysis under gravity, seismic and vertical displacement event (VDE) downward loads.

Most of the welds in the inner shell will have butt-joint configurations with both-side access and will be radiographically inspected to assure 100% weld efficiency. However, the one-sided weld joints between the outer shell and the ribs/housings, and the field joints, cannot be radiographically inspected and so will be inspected by UT. R&D is being carried out on UT inspection on one-sided 60 mm thick plate in the inner and outer shell configuration. Considering the limited access, the use of waves launched at an angle of 20° or 30° as well as 45° and 60° has been tested, as shown in Fig. 4. Regarding the surface inspection of welds, the applicability of liquid penetrant dye test (LPT) during the initial assembly phase has been assessed, and it is proposed to select suitable liquid penetrant with very low impurities (sulfur and halogen) and a limited amount of high temperature vaporization components. As a possible alternative to LPT, the Photothermal Camera method has been developed and tested. In inspections carried out on weldment surfaces from narrow gap TIG in 60 mm stainless steel, the Photothermal Camera is generally more sensitive and reliable than LPT and better discriminates linear (>1.6 mm) and rounded (>4 mm) flaws [2,3].

Thermal–hydraulic tests have been performed to confirm the VV cooling parameters for future licensing. The tests were focused on studying (Step 1) heat transfer in differently oriented and non-uniformly heated rectangular channels, (Step 2) flow distribution and stability in the parallel channels, (Step 3) development of natural circulation in the entire VV cooling circuit. The Step 1 results gave confidence in the acceptable VV cooling performance, which should provide not less than 500 $W/(m^2 K)$ heat transfer coefficient in the first channel behind the inner shell at any location in the VV [2]. For Step 2, a two-channel model (see Fig. 5) has been developed and tested. Between the inner and outer shells of the VV, the in-wall shielding plates form parallel cooling channels. Each channel is characterized by different cross-sections (the height is from 60 to 5 mm), heat loads and orientations. It is difficult to predict the flow distribution in the parallel channels at extremely low flow velocities (few mm/s). The model is a rectangular box 0.2 m wide, 3 m long, with 2.48 m heated length, and it is divided by an intermediate plate into two-channels: upper with 50 mm height and lower with 12 mm height. Three independent heaters are located at the upper, lower and intermediate walls. The test results for vertical channels showed that hydraulic friction is not dominant and that the heating rate has the dominant effect on the flow distribution especially at low flow

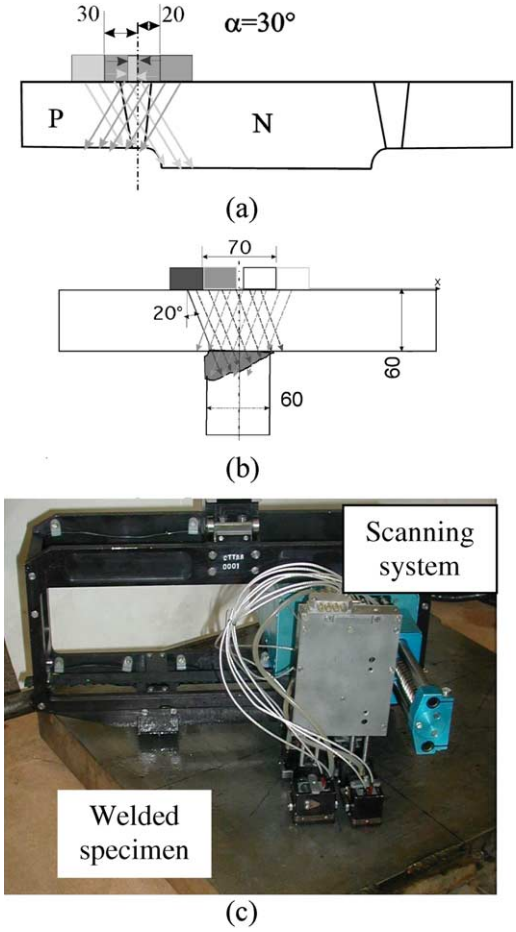

Fig. 4. UT inspection tests on welded 60 mm plates. (a) Welding for flexible support housing. (b) Welding for poloidal rib to inner shell. (c) UT inspection system during testing (RFPT).

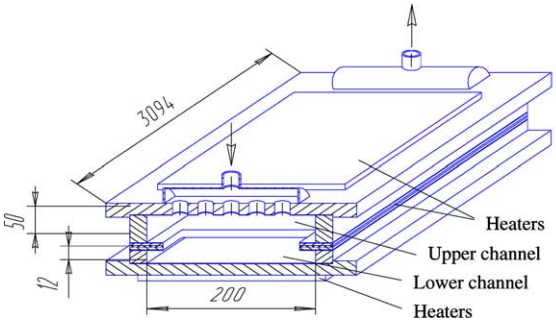

Fig. 5. Two-channel test model (RFPT).

velocity. The results will be taken into account in the VV cooling design.

2.2. Preparation of VV procurement specifications and material specifications

The main vessel, blanket coolant manifold and the port technical specification documents have been prepared in draft. The documents include a description of the scope of supply, contract stages, delivery schedule, ITER and supplier's responsibilities, and supporting documentation to be provided by the supplier. The document also lists the top level requirements and acceptance standards. A series of sketches/figures consistent with the latest vessel design are inserted into the text in order to aid understanding. The detailed information is restricted to other documents (annexes), which are referenced in the main document. These include material specifications, detailed drawings of a vessel sector (including tolerance requirements), weld qualification requirements, cleaning specifications, pressure testing, leak testing, etc. and a suggested manufacturing procedure.

Material specifications for the vacuum vessel are under preparation in close contact with possible manufacturers. These specifications are based on the ASME/ASTM specifications and additionally include ITER specific requirements such as chemical composition (reduction of the cobalt and niobium content, reduction of boron for re-welded components) and some requirements for specific properties (saturated magnetization for steel 430), etc. The specification for austenitic stainless 316L(N)-IG steel is being prepared using the extensive experience of the RCC-MR Code. Due to an optimal combination and tight specification of the main alloying elements, such as carbon, nitrogen, nickel, chromium, manganese and molybdenum, this steel has high minimum tensile mechanical properties combined with good ductility, toughness, and corrosion resistance.

3. FW/blanket design and R&D

The basic design of the FW/blanket system remains that of a modular configuration, with a mechanical attachment system to the vessel. Each blanket module consists of four FW panels and a shield block (see Fig. 6(a)). Each FW panel is fixed to a shield block with a central support beam. YAG laser welding will be used for the joint between the central support beam and the shield block. The central beam has a race-track shape with a cross-section 100 mm × 200 mm and weld thickness 6–8 mm, as shown in Fig. 6(b). The most critical forces on the FW panel and the central beam are due to halo currents. The maximum halo current on a FW panel is defined to be 48 kA as the design condition,

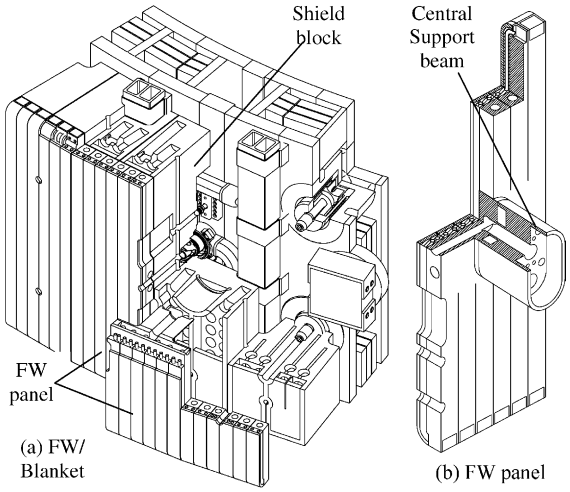

Fig. 6. Blanket module and First wall panel with a central support beam.

based on consideration on the latest plasma simulation analysis. The structural analysis shows structural integrity of the support beam with enough margin. The limit analysis results indicate that the collapse load is ~30% higher than the required value defined in the design code.

The shield block has co-axial radial cooling channels with efficient cooling of a complicated geometry on the back. Each shield block consists of 4 sub-blocks with ~23 radial holes of 45 mm diameter (see Fig. 7) [4]. The radial hole has a flow separator inside to achieve a co-axial radial coolant flow and high heat transfer coefficient. Preliminary hydraulic analysis has been performed for the shield block, and the pressure drop in the shield block is approximately 0.08 MPa.

FW R&D has been continued with the manufacture and testing of mock-ups and panel prototypes to further improve the engineering margins and to decrease the fabrication cost. It has been confirmed through R&D that FW mock-ups with Be tiles withstand a heat flux up to 2.5 $MW\,m^{-2}$ for 1000 cycles or 0.7 $MW\,m^{-2}$ for 13 000 cycles [5], which is adequate for the equivalent design requirement of 0.5 $MW\,m^{-2}$, 30 000 cycles. Four FW panel prototypes are being fabricated to demonstrate the feasibility of HIPing (Hot Isostatic Pressing) or brazing of Be to DS-Cu or CuCrZr. Three of four FW panel prototypes have been successfully completed: one made from DS-Cu Al25 with Be tiles joined onto the Cu alloy by furnace brazing at 780 °C, and the second made from CuCrZr alloy with Be tiles joined by low-temperature HIPing at 580 °C. HIP quenching (i.e. cooling rates above 40 °C/min) was performed on the CuCrZr panel to keep acceptable mechanical properties of the Cu alloy. This challenging technology was applied to the full-scale FW panel prototype for the first time.

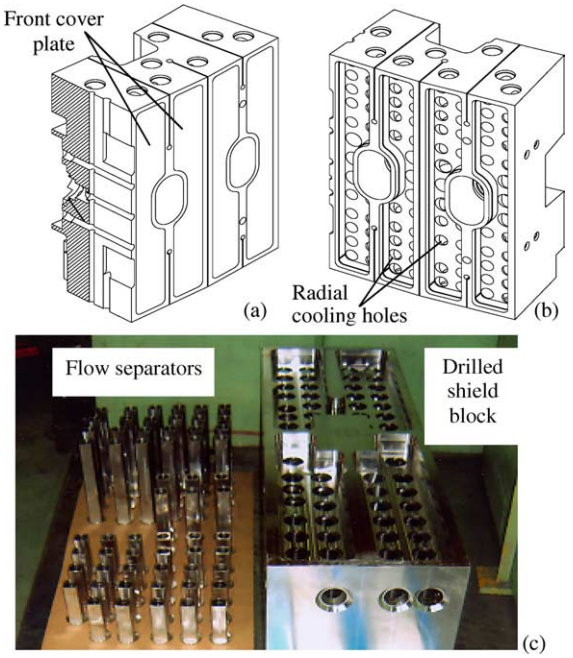

Fig. 7. Radial flow shield block structure, (a) shield block with front cover plates, (b) shield block with radial cooling holes, (c) fabrication R&D (JAPT).

The third prototype (see Fig. 8) was recently made from DS-Cu Al25 alloy with Be tiles HIPed at 730 °C and 140 MPa for 1 hour. Fifty-six beryllium tiles ($62\times62\times10$ mm) were joined onto the prototypes, and heat flux cycle testing will start at the end of this year. One more prototype is being made with powder HIPed CuCrZr and low temperature HIPed Be tiles.

It is also considered to use casting to join the CuCrZr heat sink with SS and fast brazing to join Be to CuCrZr as an alternative method of FW panel manufacturing to reduce the fabrication cost. After TIG welding of steel pipes, vacuum casting of CuCrZr was performed and followed by heat treatment: solution-annealing at 1000 °C/water quenching/550 °C – 6 h (ultimate tensile strength is 320 MPa). Fast brazing of Be tiles was carried out in high vacuum at a temperature of 700 °C. The required heating rate (~1.5 °C/s) was provided by an electron beam. To check the quality of the FW mock-up (500 $mm^{L}\times110$ $mm^{W}\times81$ mm^{t}) after casting followed by fast brazing, X-ray inspection was done. Thermal fatigue tests on the mock-up have been successfully completed up to 5000 cycles at 1 MW m^{-2} followed by 500 cycles at 1.5 MW m^{-2}. Another mock-up was manufactured to apply the same technology to the port-limiter. This mock-up (see Fig. 9) successfully withstood 2,000 thermal cycles at 7 MW m^{-2}. This result shows basic feasibility of this method for the ITER port-limiter.

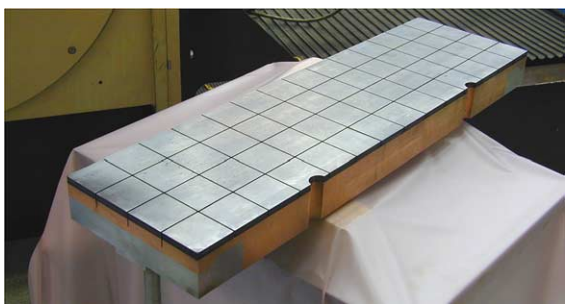

Fig. 8. Third FW panel prototype (DS Cu Al25, Be tile $62\times62\times10$ mm and HIP joint at 730 °C, 140 MPa) (EUPT).

Fig. 9. Actively-cooled Be armored mock-up with cast CuCrZr layer (successfully withstood 2000 thermal cycles at 7 MW m^{-2}) (RFPT).

Regarding the blanket module attachment system (see Fig. 10), the Ti-alloy flexible supports and CuCrZr electrical connectors have been fabricated and tested [6]. Fabrication and testing is underway for prototypes of the flexible support as a complete system including the housing, which is a part of the vessel (see Fig. 11). The test conditions are defined to simulate the EM loads and thermal displacements. The axial load is ±500 kN, the lateral displacement is ±1 mm, and the angular displacement is 3 mrad. A fatigue test up to 300 cycles for each condition has been completed, and no changes or plastic deformations were observed.

For the hydraulic connection from the blanket module to the manifold, a co-axial pipe connection with guard vacuum for leak detection has been designed and tested (see Fig. 12). The outer welds are in 3.75 mm thick, 100 mm diameter pipe. A 4 kW NdYAG laser was selected for welding and cutting and a special tool developed to achieve a front access through the blanket module. The tool transfers the laser power via parallel optics to allow for visual examination of the weld before and during welding and cutting operations. For high quality cutting of the 100 mm diameter tube, it is necessary to bring a powerful jet of gas close to the cut surface and this is reliably and safely achieved in this tool by means of a nozzle that flips out when an outer

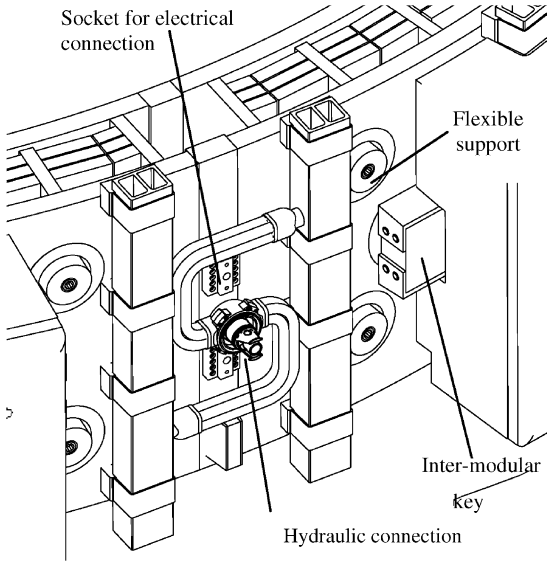

Fig. 10. Blanket module attachments (hydraulic connection, Inter-modular keys, toroidal key, flexible support, sockets for electrical connection).

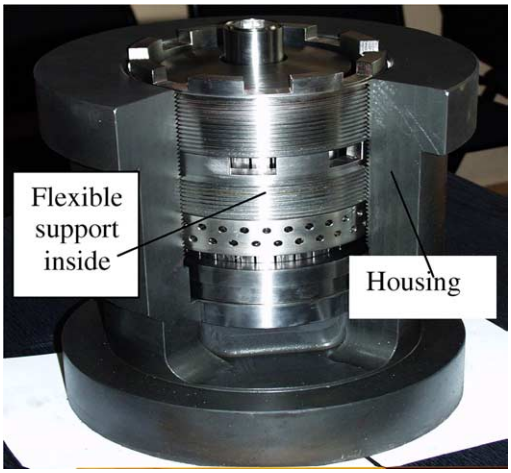

Fig. 11. Cycle load testing of blanket flexible support and housing (RFPT).

tube is retracted. During welding, a different nozzle with a cross-jet is needed to protect the optics from damage by spatter from the weld. Cutting of the tubes is successful with about 0.5 mm roughness, but with adherence of globules of metal to the rear side. Successful autogenous welds were achieved on cleanly prepared edges with good fit-up and, in order to investigate the possibility of replacement rewelding without an intermediate machining operation, attempts were made to weld clean cut surfaces to laser cut surfaces. These were less successful due to the roughness and rear side

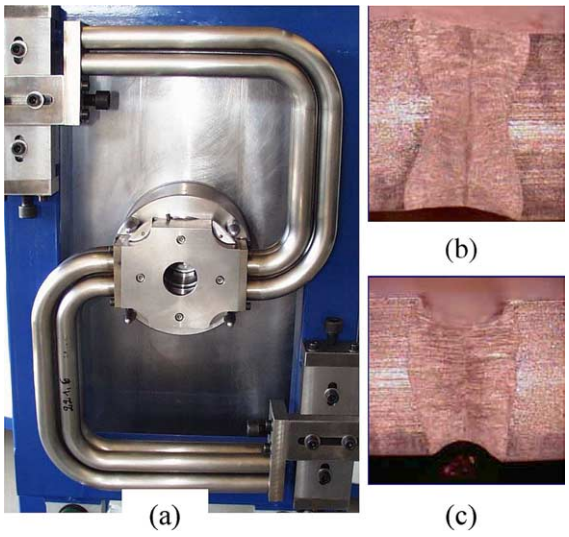

Fig. 12. Fabrication and testing of co-axial hydraulic connection for blanket module (EUPT). (a) Co-axial hydraulic connection model, (b) with two machined edges, (c) laser cut edge to machined edge.

adhesion and weld defects such as undercut and cracks were identified. These process trials will be extended to a mock-up of the complete unit. Weld surface crack and defect detection experiments, using eddy current and laser crack detection, and vacuum leak detection principle tests, are also in progress.

4. Divertor design and R&D

The ITER divertor consists of 54 cassettes onto which are mounted replaceable plasma-facing components (PFCs). Carbon–fibre composite (CFC) armour is preferred for the regions of the PFCs where the SOL strikes the targets and the design heat flux is 20 $MW\,m^{-2}$, and tungsten for all other plasma-facing surfaces of the PFCs. The CFC monoblock geometry, which has a capability up to $\sim$30 $MW\,m^{-2}$ and has no cases recorded of tiles detaching, is maintained as the preferred option, in preference to a flat tile geometry, which sometimes exhibits failure leading to complete tile detachment at 18–20 $MW\,m^{-2}$. For the W armoured surfaces, where the heat flux <5 $MW\,m^{-2}$, both flat tile and monoblock geometries are suitable, having sustained up to 27 and 18 $MW\,m^{-2}$, respectively.

The manufacture of CFC monoblock and W lamellae armour on the same PFC has been demonstrated on prototypical elements (see Fig. 13) with the armours joined via a cast pure Cu layer to a CuCrZr tube by low temperature HIP. HIP joining of pure Cu to CuCrZr tube at 550 °C produces optimum mechanical properties in the CuCrZr and a grain size <200 μm [7]. Under high

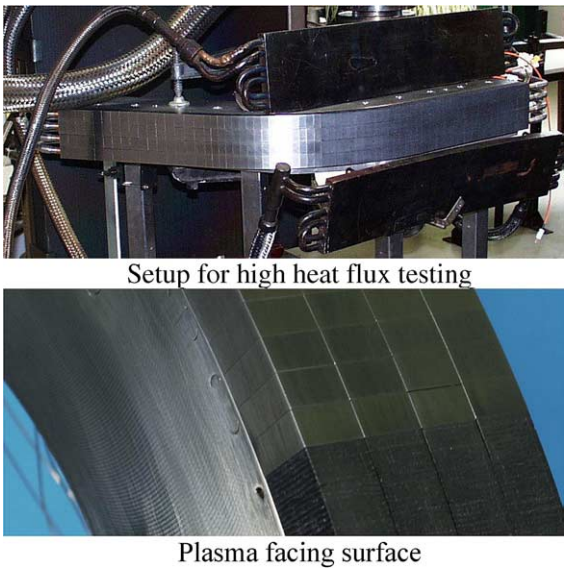

Fig. 13. Prototypical vertical target (EUPT).

heat flux (HHF) testing the CFC armour has survived 1000 cycles at 20 MW m^{-2} and the W lamellae 700 cycles at 10 MW m^{-2}.

An extensive radiation campaign (see Table 1) has been carried out and these results support the armour geometry choices described above.

It has been demonstrated that an acceptable pressure drop and a similar CHF to that of a conventional swirl tube can be obtained using an annular flow coolant tube (see Fig. 14) [8]. A CFC-monoblock-amoured mock-up was produced using 15Cu–25Ni–60Ti braze for the CFC/OFHC Cu joint and 52Cu–10Ni–38Mn for the OFHC-Cu/CuCrZr tube joint, both brazed in the same cycle at 980 °C and gas quenched by Ar at 1 °C s^{-1} to maintain good mechanical properties in the CuCrZr. After brazing, initial cracks observed in the CFC side wall were not observed to grow and there was no degradation of thermal performance during HHF testing during 1000 cycles at 20 MW m^{-2}.

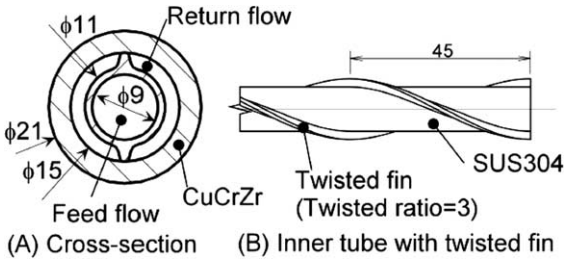

Fig. 14. Detail of annular flow coolant tube (JAPT).

Efforts have also been focused on PFCs using the hypervapotron cooling technique, which keeps the Cu-armour interface <500 °C during operation and hence, is suitable for W flat tile armour. The elements are built by casting CuCrZr onto stainless steel, followed by rolling to obtain a 12% reduction of the bi-metal plate giving a finer grain structure and improved tensile strength. The hypervapotron ribs are formed by machining through the steel into the CuCrZr and all subsequent joints in the substrate are steel to steel. The W armour tiles are pre-coated with a cast pure Cu layer before being brazed using CuInSnNi alloy to the CuCrZr in a fast braze cycle. A 0.6 m long mock-up of this design withstood a HHF test of 1000 cycles at ~20 MW m^{-2}. Two similar mock-ups are under construction. CuCrZr explosively bonded to stainless steel 316 LN has successfully undergone mechanical and helium leak tests and will be armoured with both CFC and W, using HIPing and brazing, respectively.

The potential for large quantities of tritium to be trapped through co-deposition with sputtered carbon has long been a concern. Experiments [9,10] indicate that the deposition of hydrocarbons and the survival of hydrocarbon radicals in the pumping ducts beneath the divertor should be negligible due to the high ratio of atomic hydrogen to hydrocarbons, the high density in the divertor and the general surface temperature >100 °C. Only stable hydrocarbon species will reach the cryopumps where they will be processed in the normal

Table 1
Results from recent irradiation campaign (EUPT)

Description	dpa	Irradiation temperature (°C)	Conditions (values are for absorbed heat flux)	Results
W monoblock	0.1	200	1000 cycles @ 18MW m^{-2}	No failure
W monoblock	0.5	200	1000 cycles @ 18MW m^{-2}	No failure
W flat tile 5×5×6	0.1	200	1000 cycles @ 10 MW m^{-2}	Loss of tile
W flat tile 5×5×6	0.5	200	1000 cycles @ 10 MW m^{-2}	Overheating
CFC monoblock	0.2	200	1000 cycles @ 12 MW m^{-2}	No failure, test stopped[a]
CFC monoblock	0.35	350	1000 cycles @ 15 MW m^{-2}	No failure
CFC flat tile	0.2	200	1000 cycles @ 19.5 MW m^{-2}	Loss of tile

[a] Due to high surface temp caused by lower irradiated CFC thermal conductivity.

Table 2
Selected materials for the ITER vacuum vessel and in-vessel components

Plasma facing materials	Blanket first wall	Sintered beryllium plates or plasma spray beryllium
	Divertor target	Carbon–fiber composite (CFC) – 3D
	Other divertor areas	Pure tungsten rolled plates
High thermal conductivity layer		CuCrZr, DS Cu, pure copper as compliant layer
Structural materials		Austenitic steel 316 L(N)-IG, austenitic steel 304(L)
In-wall shielding for the vacuum vessel		Borated steel 304B4/B7 and ferritic steel 430 (for ferromagnetic insert)
Blanket flexible support		Ti alloy Ti–6Al–4V mill annealed
Fastening bolts	Blanket support	Nickel alloy 718
	Port plug flange	Nickel alloy 718, precipitation hardened steel 660
Blanket module electrical connector		CuCrZr plates
Pads for the keys		CuCrZr or aluminum bronze
Electrical insulation layer		Plasma-sprayed Al_2O_3 or $MgAl_2O_4$

manner. However, experiments are still studying the possibility of long chain CxHy (e.g. octane) reaching the activated charcoal surfaces of the cryopumps where they will permanently impair pumping efficiency.

Elsewhere in the divertor and in the main chamber, the tritium co-deposition rate is even less certain, and in the absence of an experiment with the ITER mix of wall materials is likely to remain so. Hence, during initial operation of ITER, regimes will need to be identified which minimize erosion of carbon and its co-deposition with T, and/or techniques developed to remove the deposits. A backup solution may be to move to an all-metal divertor.

5. Summary of material selection

The main materials for the VV and in-vessel components have been selected [11], and further refined as summarized in Table 2.

6. Conclusions

The design and fabrication methods of the ITER nuclear components have been confirmed by the R&D, and alternate fabrication methods have also been shown to be feasible. The nuclear component design and R&D have progressed significantly in detail in collaborative efforts between the International Team and the Participant Teams, and the development of procurement specifications for long lead items is making good progress.

References

[1] K. Ioki et al., Nucl. Fusion 41 (3) (2001) 265.
[2] K. Ioki et al., Nucl. Fusion 43 (2003) 268.
[3] L. Jones et al., in: Proceedings of the 22nd Symposium on Fusion Technology, Helsinki, 2002, in press.
[4] Y. Kosaku et al., Fabrication of prototype mockups of ITER shielding blanket with separable first wall, JAERI-Tech 2002-063, 2002.
[5] P. Lorenzetto et al., Fusion Eng. Des. 61&62 (2002) 643.
[6] K. Ioki et al., Fusion Eng. Des. 61&62 (2002) 399.
[7] M. Merola et al., Fusion Eng. Des. 66&68 (2003) 211.
[8] K. Ezato et al., Fusion Sci. Technol., in press.
[9] I. Arkhipov et al., J. Nucl. Mater. 313–316 (2003) 342.
[10] G. Fuesmann, IPP Max-Planck-Institut fur Plasmaphysik, Berlin, June 2002, private communication.
[11] K. Ioki et al., J. Nucl. Mater. 258–263 (1998) 74.